University of Thi-Qar Journal Vol.12 No.3 SEP 2017
Web Site: https://jutq.utq.edu.iq/index.php/main
Email: journal@jutq.utq.edu.iq

The Numerical Prediction of Flow of Branched Polymer Melts Through Planar Contraction Channel by Finite Element Method

https://doi.org/10.32792/utq/utj/vol12/3/1

H.A. Khalaf
Thi-Qar University, Thi-Qar, Iraq,
eng.hussam@mail.ru

Abstract

In this work we present an investigation of a complex viscoelastic flow through an abrupt expansion with expansion ratio D/d = 4, where the Oldroyd-B model was consider as a constitutive equation. The governing equations are solved using the Finite Element Method. The polymer is modeled as a monodisperse suspension of "Oldroyd-B" molecules, which provides a direct link the molecular topology and the flow properties of the melt. The branching produces an enhancement in the size of upstream vortex in creeping flows. Also was found that including inertia forces will give the intensity of lip vortex increases, while the size of corner vortex will initially decreased with growth of Weissenberg number but with more increase (We>4), the size of corner vortex will begin to increase in size. The effect arises from the differing responses in shear and extensional flows of polymer melts.

Keywords: viscoelastic flow, Oldroyd-B, Rheology, Weissenberg number, Planar Contraction Channel, lip-vortex, Finite Element method.

Introduction:

The focus of this paper is on the prediction of the flow of branched polymer melts through a 4:1 planar contraction using the Oldroyd-B model of

Crispulo Gallegos [1].There have been many extensions to the tube kinetic model for entangled melts developed by Doi and Edwards [2], including the DCR model of Marrucci [3], the pom-pom model of McLeish and Larson [4], as well as versions of the extended pom-pom model [1]. These models have two characteristics that are missing from phenomenological models such as the Oldroyd-B model. The first characteristic shows how the melt rheology is dependent on the molecular structure of the polymer, while the second one indicates that the spectrum of relaxation times leads to partial differential equations for the orientation and stretch. The original pom-pom model of McLeish and Larson [4] is based on an idealized polymer molecule in which the polymer chains are represented by a backbone segment connecting two identical pom-poms each with q arms at the branch points. The drag that the melt spend on these arms leads to stretching the back bone. The branch points slow down the reprated motion of the backbone by pinning the molecule in place at the tube junctions. The free ends of the arms are still able to move, however, and the polymer is able to free itself from the tube by a process known as arm-retraction, which is triggered when the molecule reaches its maximum stretched state. The arms progressively move their way outof the tubes towards the branch points by diffusion. Once the arms relax, the backbone can subsequently relax by moving the branch points. The finite extensibility constraint on the backbone stretch gives rise to discontinuity in the gradient of the steady-state extensional viscosity. Blackwell et al. [5] adjusted the evolution equation for the stretch to allow for branch point displacement. These effects by removing the discontinuity in steady-state extensional viscosity gradient. The two remaining major drawbacks in the original pom-pom model, viz. the prediction of a zero second normal stress-difference and the unboundedness of the backbone orientation equation, were addressed in the extended pom-pom (XPP) model developed by Verbeeten et

al. [1]. Because it was adopted as a benchmark problem at the 5th international workshop on numerical methods in non-Newtonian flows [6], the planar 4:1 contraction problem has been at the forefront of computational rheology. It is currently considered that the choice of 4:1 contraction ratio is limiting with respect to stimulation of a rich variety of interesting flow phenomena. Aremarkable exception to the lure of the 4:1 configuration is the recent paper of Alves et al. [7] who investigated the effect of varying contraction ratio on creeping flow characteristics in a planar contraction for a linear Phan-Thien/Tanner (PTT) fluid ($\varepsilon = 0.25$), capable of moderate strain-hardening. Nevertheless, due to the inclusive literature on the 4:1 contraction problem it is still important benchmark problem on which to test the accuracy and stability of numerical schemes. A comprehensive account of experimental observations and numerical predictions is presented in the research monograph of Owens and Phillips [8] and the review paper of Evans and Walters [9]. We finish with some introductory remarks, reporting on some of the contributions that have been made to the understanding of this subject [12].

The main objectives of the present study are: (i) to investigate effects of non-dimensional parameter (We) of the Oldroyd-B model upon the flow for a planar sudden expansion of lower expansion ratio of 1:4; (ii) to analyse the effect of elasticity on the flow field; (iii) to show the variation of profiles of the velocity and shear stress along the centerline for the Newtonian and viscoelastic cases.

Numerical simulation:

In the present work we consider the two-dimensional incompressible, isothermal flow from a straight channel of height d to the width of the expanded channel D, corresponding to an expansion ratio E, (E=D/d=4) as shown in Fig.1. Fluid passes from one channel into another of smaller cross-

sectional width and in the process generates a complex flow exhibiting regions of strong shearing near the walls and uniaxial extension along the centerline. In the literature on viscoelastic contraction flows, interest has focused amongst other things upon the following vortex behaviour, pressure drop across the contraction and velocity overshoot along the axis of symmetry.

Under the above assumptions the governing equations comprise the conservation equations of momentum and mass, together with a rheological equation of state. In this paper the single equation version of the extended Oldroyd-B model is considered. The equations of motion and continuity are [10]:

$$\rho\left(\frac{\partial v_i}{\partial t}+v_j\frac{\partial v_i}{\partial x_j}\right)=-\frac{\partial P}{\partial x_i}+\frac{\partial \tau_{ij}}{\partial x_j}+\mu_s\frac{\partial^2 v_i}{\partial^2 x_j},\qquad \frac{\partial v_i}{\partial x_i}=0,$$

(1)

where v_i is the velocity field, ρ is the density, μ_s is the solvent viscosity, p is the pressure and τ_{ij} is the polymeric contribution to the extra-stress tensor. The constitutive equation for the single equation version of the Oldroyd-B is [10-13], [16-17]:

$$f(\lambda,\tau_{ij})\tau_{ij}+\lambda_{0b}\frac{\delta\tau_{ij}}{\delta t}+G_0[f(\lambda,\tau_{ij})-1]I_{ij}+\frac{\alpha}{G_0}\tau_{ij}\cdot\tau_{ij}=2\lambda_{0b}G_0 D_{ij},$$

(2)

$$\frac{\delta\tau_{ij}^V}{\delta t}=\frac{\partial\tau_{ij}^V}{\partial t}+v^k\frac{\partial\tau_{ij}^V}{\partial x^k}-\frac{\partial v_k}{\partial x_i}\tau_{kj}^V-\tau_{ik}^V\frac{\partial v_k}{\partial x_j},$$

(3)

$$f(\lambda,\tau_{ij})=\frac{\lambda_{0b}}{\lambda_{0s}}\left(1-\frac{1}{\lambda}\right)e^{\upsilon(\lambda-1)}+\frac{1}{\lambda^2}\left[1-\frac{\alpha I_{\tau_{ij}\cdot\tau_{ij}}}{3G_0^2}\right]$$

(4)

In these equations, λ_{0b} and λ_{0s} represent the orientation and backbone stretch relaxation times, respectively, and G_0 is the linear relaxation modulus.

The parameter ν in (3) was incorporated into the model to remove the discontinuity in the derivative of the extensional viscosity that was present in the differential approximation of the original pom-pom model. Its value is estimated by data-fitting and found to be inversely proportional to the number of arms q. More precisely, we have $\nu = \frac{2}{q}$. Finally, the extra-stress tensor can be written as the sum of polymeric and solvent contributions, i.e.

$$T_{ij} = \tau_{ij} + 2\mu_s D_{ij}$$

(5)

The governing equations are made dimensionless by scaling length by L, velocity by U, time by L/U and pressure and extra-stress by $\mu U/L$, where $\mu = \mu_S + \mu_P$ is the total viscosity. To preserve similarity between the form of the nondimensional Oldroyd-B model, we define $\mu_P = G_0 \lambda_{0b}$. Then, defining dimensionless parameters Re, We, β and ε, viz.

$$\mathrm{Re} = \frac{\rho U L}{\mu}, \quad We = \frac{\lambda_{0b} U}{L}, \quad \beta = \frac{\mu_S}{\mu_S + G_0 \lambda_{0b}}, \quad \varepsilon = \frac{\lambda_{0b}}{\lambda_{0s}}$$

(6)

where Re=Reynolds number, We=the Weissenberg number, β=the solvent viscosity ratio, ε=the ratio of the stretch to orientation relaxation times.

The governing equations may be transformed into non-dimensional form,

$$\mathrm{Re}\left(\frac{\partial v_i}{\partial t} + v_j \frac{\partial v_i}{\partial x_j}\right) = -\frac{\partial P}{\partial x_i} + \frac{\partial \tau_{ij}}{\partial x_j} + \beta \frac{\partial^2 v_i}{\partial^2 x_j}, \qquad \frac{\partial v_i}{\partial x_i} = 0,$$

(7)

$$f(\lambda,\tau_{ij})\tau_{ij}+We\frac{\delta\tau_{ij}}{\delta t}+\frac{(1-\beta)}{We}[f(\lambda,\tau_{ij})-1]I_{ij}+\frac{\alpha We}{(1-\beta)}\tau_{ij}\cdot\tau_{ij}=2(1-\beta)D_{ij}, \quad (8)$$

$$f(\lambda,\tau_{ij})=\frac{2}{\varepsilon}\left(1-\frac{1}{\lambda}\right)e^{\upsilon(\lambda-1)}+\frac{1}{\lambda^2}\left[1-\left(\frac{We}{(1-\beta)}\right)^2\frac{\alpha}{3}I_{\tau_{ij}\cdot\tau_{ij}}\right]$$

$$\lambda=\sqrt{1+\frac{We}{(1-\beta)}\frac{1}{3}I_{\tau_{ij}}} \quad (9)$$

The extra-stress tensor T_{ij}, is given by $T_{ij}=\tau_{ij}+2\beta D_{ij}$. The parameter ε, the ratio of the stretch to orientation relaxation times, is inversely proportional to the entanglement molecular weight of the backbone segments. Values of ε approaching unity correspond to molecules with relatively short backbone lengths but long arms to slow down the dynamics. Small values of ε correspond to highly entangled backbones.

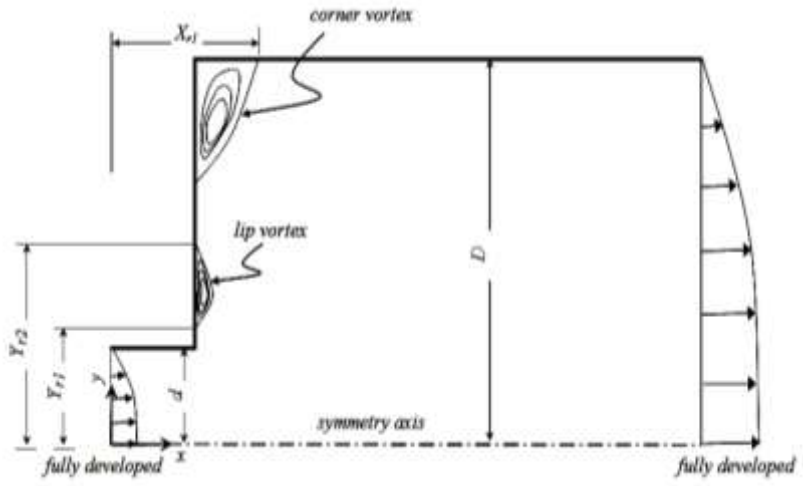

Figure (1): Schematic representation of the 1:4 planar sudden expansion.

The boundary conditions are set according to the following:

- A fully-developed (Poiseuille axial-velocity profile) at the inlet and the outlet of the channel.

- On the walls, no-slip boundary conditions are applied:

$$u = 0 \; ; \; v = 0 \qquad \ldots \ldots (10)$$

- At the inlet of the channel, the axial and the radial velocity components are set as:

$$u(y) = 1.5U\left[-\left(\frac{y}{h/2} \right)^2 \right] \; ; \; v = 0 \qquad \ldots \ldots (11)$$

- At the outlet of the channel, the axial and the radial velocity components are set as:

$$\partial u/\partial y = 0 \; ; \; \partial v/\partial y = 0 \qquad \ldots \ldots (12)$$

- The inlet and outlet values of pressures are extrapolated depending on the inflow pressure value.

Mixed finite element formulations:

Consider the steady, incompressible flow of an viscoelastic fluid. As a point of departure the classical three-field mixed formulation is chosen, in which, besides the momentum and continuity equation, the constitutive equation is also cast in a weighted residuals form. This is a natural extension of the common velocity-pressure formulation for Stokes type problems and implicitly accounts for the partial differential form of the constitutive equation. We consider a triangular discretization of the domain, choose the quadratic polynomial approximation of the velocities v_i plus linear approximation of the pressure. Regarding the extra-stress tensor τ_{ij}, a continuous linear or quadratic interpolation has been chosen. After discretization of the set of eqs. (1)–(2), we have to solve a non-linear algebraic system. At least, two basic approaches may be adopted to handle

this non-linearity, a decoupled and a coupled one. In the decoupled approach, the computation of the viscoelastic extra-stress tensor is performed separately from that of the flow kinematics by splitting the global system into two sub-systems: the conservation equations (equ. (1)) and the evolution equation of the extra-stress tensor equ. (3). From known kinematics (v_i and p), one calculates the tensor τ_{ij} solution of equ. (3). The kinematics are then updated by solving the conservation equations. The iterative procedure is generally based on Picard's iteration scheme. This approach has been used by several authors. (see Aboubacar et al. [6] and Béraudo C., et al. [14]).

Results and Discussion:

Numerical result have been obtained by pursuingthe following values the non-dimensional parameters: $\varepsilon = 1/3, q = 2, \alpha = 0.15$ and $\beta = 1/9$. Calculations have been done for Weissenberg numbers in the range $0 \le We \le 20$ and the value of the Reynolds number have been taken in consideration, viz. $\mathrm{Re} = 5$. In Fig. 3, the obtained results for the constant-viscosity Oldroyd-B model are presented in terms of streamline plots, to increase Weissenberg numbers in the range $0 \le We \le 6$. The results present a diminishing corner vortex and the appearance and enhancement of a tiny lip vortex with an increase in the elasticity (We). when We=0, there is just the vortex at the salient corner. Lip vortex enhancement could be indicated as We increases. As We increases, the intensity of lip vortex increases as well, while the size of corner vortex decreases. At We = 2 A minute lip vortex is barely can be seen and is very close to the re-entrant corner and it grows in size as We increases but cannot be visible when We is less than 2. This behaviour is in agreement with the previous results of Aboubacar and Webster [6] and Alves et al. [7], which obviously predicts the shrinking of

the corner vortex up to We=4 and the appearance of a lip vortex at We=2.When We=6, the both vortex (corner, lip) will be mixed and get to be one large vortex.

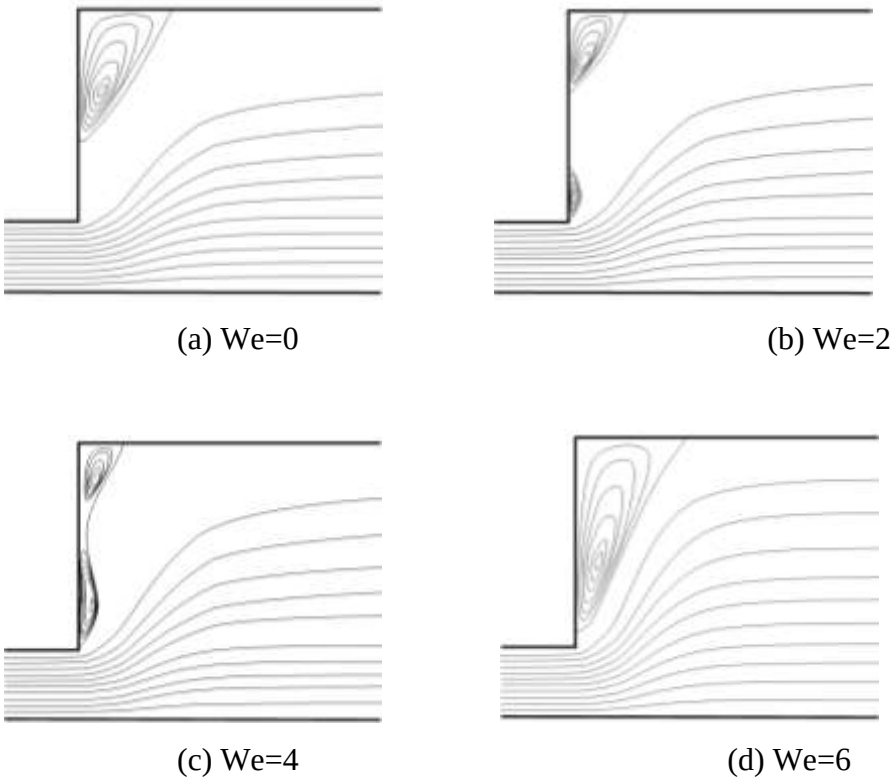

(a) We=0 (b) We=2

(c) We=4 (d) We=6

Figure (2): Streamline patterns for an Oldroyd-B fluid Stream function with increasing We, Re=5.

a) We=0, b) We=2, c) We=4, d) We=6

To study the effect of a mesh refinement on numerical results, we used Richardson's extrapolation method and have been three computational mesh as given in Table (1). The mesh-converged value is given as [15]:

$$\Phi = \frac{\left(N_3/N_2\right)^{OS}\Phi_3 - \Phi_2}{\left(N_3/N_2\right)^{OS} - 1} \quad \ldots \ldots (13)$$

and the relative error as:

$$E_r = \left|\frac{\Phi_3 - \Phi}{\Phi}\right| \times 100 \quad \ldots \ldots (14)$$

where Φ_3 and Φ_2 are values of particular flow variables corresponding to a Mesh M3 and Mesh M2. N_3 and N_2 represents the number of elements for Mesh M3 and Mesh M2.

We use a mesh independence test for verification of the accuracy of the results by taking the three computational mesh 1000×140, 1200×150 and 1400×160. Tables (1) shows the accuracy of data for recirculation lengths and the separation point (Xr_1) on the upper walls for We=2 and Re=5.

Computational grid at the channel is represent as in Fig.3, which became coarser at the center of channel while close to the walls the grid was finer. The Meshes M3, M2 and M1 are agree well. The estimated numerical accuracy for recirculation lengths equal to Er=0.0196% for Xr_1 for M3. In Fig.4 show distribution of axial velocity on center x-line for different grids (M1, M2 and M3) with We=2 and Re=5. and we can observe the convergence of the results too therefore in the end of this test we chose the mesh M3 (1400×160) for all calculations in this work.

Table (1): Effect of mesh refinement for Newtonian fluid with We=2 and Re=5.

Mesh	Number of elements	Iterations	(Xr_1)		
			Xr_1	Φ	Er[%]

M1	1000 × 140	800	3.7238	----	----
M2	1200 × 150	800	3.7245	3.72557	0.0288
M3	1400 × 160	800	3.7249	3.72563	0.0196

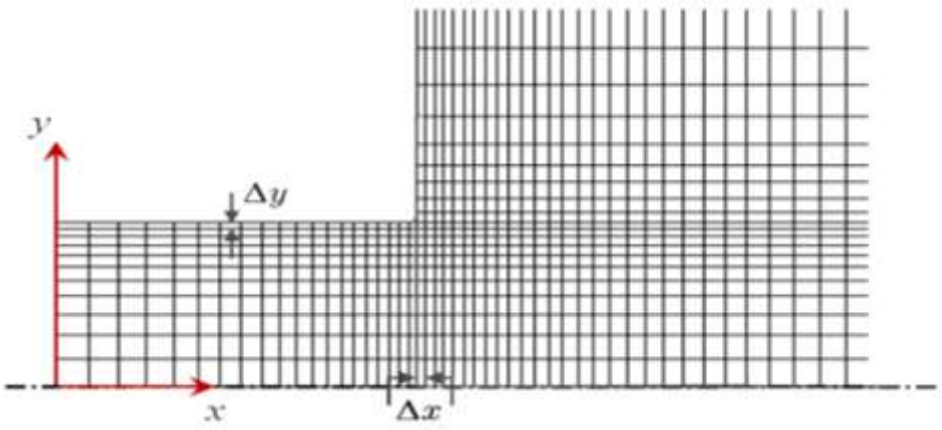

Figure (3): The fine mesh (M3) used in the calculations.

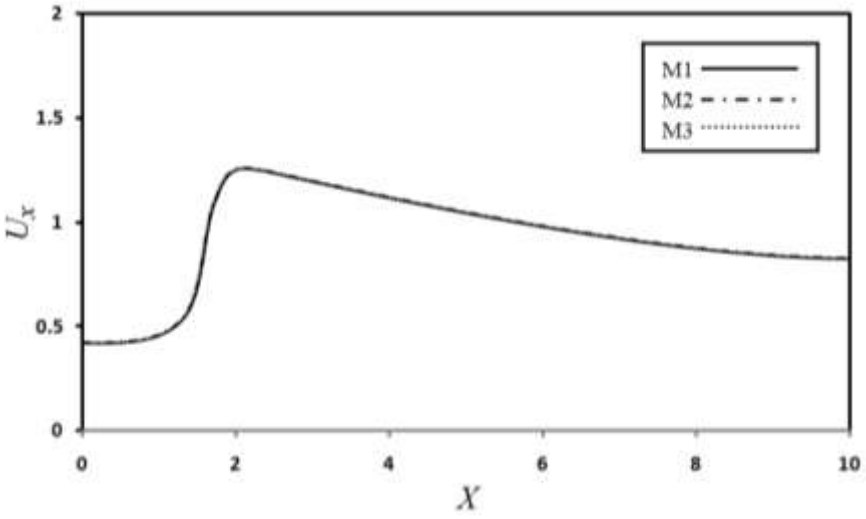

Figure (4): Distribution of axial velocity on center x-line for different grids (M1, M2 and M3) with We=2 and Re=5.

In Fig.5, the size of the corner-vortex (Xr_1) is plotted against We. This plot replicates quantitatively and shows more clearly the trend depicted by the flow patterns in Fig. 2. An initial steep rise in the vortex size is seen at We = 2, which becomes saturated asymptotically afterwards at higher We. With the introduction of inertia, we can discern vortex reduction with increasing Weissenberg number. This lies in dramatic contrast to the situation for creeping flow, where the vortex grows steadily in size with increasing Weissenberg number.

Initially, the size of the salient-corner vortex (Xr_1) slightly decreases up to We=4. After that, size of the salient-corner vortex (Xr_1) increases significantly until it reaches We=9 and when the Weissenberg number is increased (We>9), the increase in size of the corner vortex will be very few.

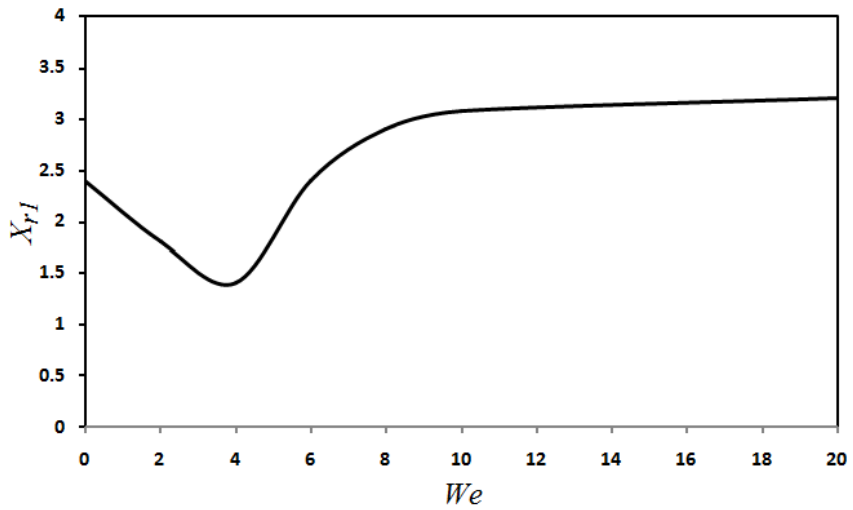

Figure (5): Effect of Weissenberg number (We) for the Oldroyd-B fluid on the size of the corner-vortex (Xr_1) on center x-line with Re=5 and mesh (M3).

The axial velocity on center x-line for different Weissenberg number is shows in Fig. 6, The streamwise velocity component along the centerline is

presented, where the velocity overshoot is so apparent with increasing elasticity and the velocity profiles seems to be nearly independent of mesh resolution. Since elongational flow is dominant along the centerline, the acceleration of velocity can be attributed to the sharp gradient of longitudinal normal stresses. The trend shows an increasing streamwise velocity with elasticity. The plots also show identical characteristics with similar plots obtained by Alves et al. [6]. The maximum velocities are predicted just inside the downstream channel, which indicates the position of highest strain along the centerline. Immediately downstream, this maximum strain is not sustainable by the shear-dominated flow and the polymer relaxes relatively quickly after a distance of about 6 widths of the downstream channel. The length of channel required for the relaxation process after the stretching of the polymer increases with Weissenberg number, which may be determined by evaluating the axial velocity gradient, along the centerline of the downstream channel.

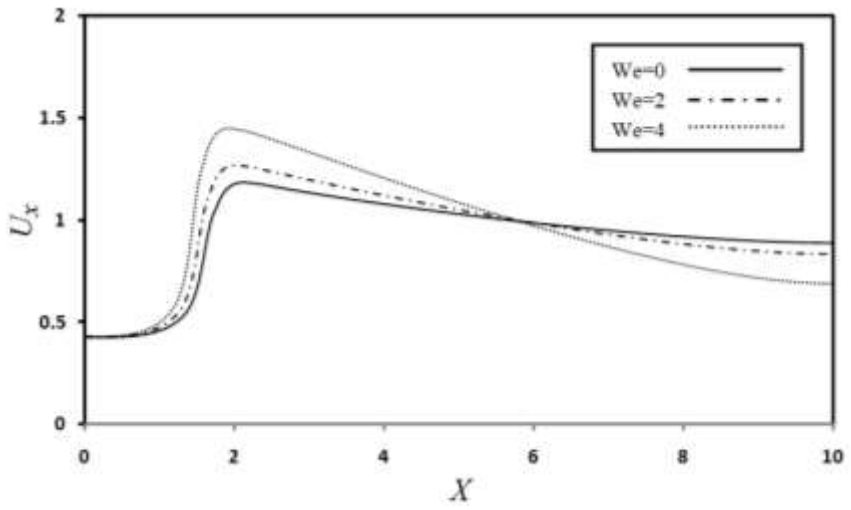

Figure (6): Effect of Weissenberg number (We) for the Oldroyd-B fluid on the axial velocity (U_x) on center x-line with Re=5 and Mesh (M3).

Fig.7 shows distribution of shear stress (T_{xy}) along the centerline of x-axis with an increase in the elasticity (We). This distribution become oscillatory in the expanded channel, and with increasing elasticity (We), this oscillatory decreases and become constant. The peak value of the extra stress increases with increasing Weissenberg number (We), which can be attributed to the existence of singularity near the re-entrant corner.

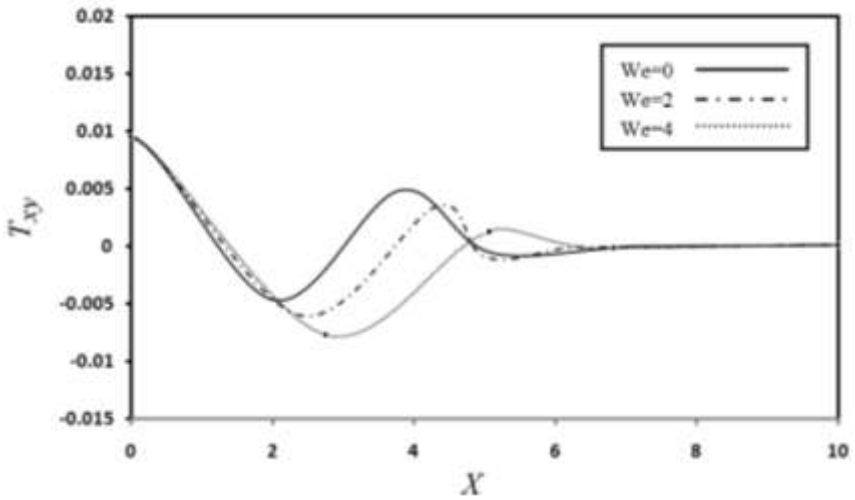

Figure (7): Effect of Weissenberg number (We) for the Oldroyd-B fluid on the shear stress (T_{xy}) on center x-line with Re=5 and Mesh (M3).

Conclusions:

Comprehensive numerical simulations with a Finite-Element Method of Oldroyd-B viscoelastic flow through Planar Contraction Channel of varying in the elasticity (We), from 0 up to 20, produced results for the vortex characteristics and the formation mechanism similar to those found in a previous studies for the planar case. The vortex type (corner, lip or mixed) is quantified in a two dimensional map with Weissenberg number (We) as independent parameter. For creeping flow, the intensity of lip vortex has been

found to increase with increasing Weissenberg number while the size of corner vortex initially decreases but with more increase (We>4), the size of corner vortex will begin to increase in size. The presence of inertia has the opposite effect on vortex intensity, which decreases with increasing Weissenberg number. With more increase (We>6), the both vortex (corner, lip) will be mixed and get to be one large vortex.

References

1. Crispulo Gallegos "Rheology" EOLSS Publications Co. Ltd, United Kingdom, Vol.1, 2010.
2. Doi M., Edwards S.F. "The theory of polymer dynamics" Oxford University Press, Oxford, 1986.
3. Marrucci G. "Dynamics of entanglements: a non-linear model consistent with the Cox-Merz rule" Journal of Non-Newtonian Fluid Mechanics, 1996, V.62, Pp.279-289.
4. McLeish T.C.B., Larson R.G. "Molecular constitutive equations for a class of branched polymers: The pom-pom model" Journal of Rheology, 1998, V.42, Pp.81-110.
5. Blackwell R. J., McLeish T. C. B., Harlen O. G. "Molecular drag-strain coupling in branched polymer melts" Journal of Rheology, 2000, V.44, Pp.121-136.
6. Aboubacar M., Phillips T.N., Snigerev B.A., Webster M.F. "High –order finite volume methods for viscoelastic flow problems" Journal of Computational Physics, 2004, V.199, Pp.16-40.
7. Alves M.A., Pinho F.T., Oliveira P.J. "Effect of a high-resolution schemes on finite volume predictions of viscoelastic flows" Journal of Non-Newtonian Fluid Mechanics, 2000, V.93, Pp.287-314.
8. Owens R.G., Phillips T.N. Computational Rheology, Imperial College Press, London, 2002.

9. Evans R.E., Walters K. "Further remarks on the lip-vortex mechanism of planar contraction flows" Journal of Non-Newtonian Fluid Mechanics, 1989, V.32, Pp.95-105.
10. Aguayo J.P., Phillips P.M., Phillips T.N., Tamaddon-Jahromi H..R., Snigerev B.A., and Webster M.F. "The numerical prediction of planar viscoelastic contraction flows using the pom-pom model and higher-order finite volume schemes" Journal of Computational Physics, 2007, V.220, Pp.586-611.
11. Al-Muslimawi A., Tamaddon-Jahromi H.R., Webster M.F. "Simulation of viscoelastic and viscoelastoplastic die-swell flows" Journal of Non-Newtonian Fluid Mechanics, 2013, V.191, Pp.45-56.
12. Choi, Y.J., Hulsen M.A., Meijer H.E.H., "Simulation of the flow of a viscoelastic fluid around a stationary cylinder using an extended finite element method", Computers and Fluids, 2012, V.57, Pp.183-194.
13. Wilco M.H. Verbeeten.,.Gerrit W.M. Peters. Frank P.T. Baaijens "Numerical simulations of the planar contraction flow for a polyethylene melt using the XPP model" Journal of Non-Newtonian Fluid Mechanics, 2004, V.117, Pp.73-84.
14. Béraudo C., Fortin A., Coupez T., Demay Y., Vergnes B., Agassant J.F., "A finite element method for computing the flow of multi-mode viscoelastic fluids: comparison with experiments", Journal of Non-Newtonian Fluid Mechanics, 1998 , V.75, Pp.1-23.
15. Ternik, P. "Symmetry Breaking Phenomena of Purely Viscous Shear-Thinning Fluid Flow in a Locally Constricted Channel", International Journal of Simulation Modelling, 2008, V.4, Pp.186-197.
16. Vazquez, P.A., Castellanos A., "Numerical simulation of EHD flows using Discontinuous Galerkin Finite Element methods" Computers and Fluids, 2013, V.84, Pp.270-278.

17. Aguayo J. P., Phillips P. M., Phillips T. N., Tamaddon-Jahromi H.R., Snigerev B. A., Webster M. F., "The Numerical Prediction of Planar Viscoelastic Contraction Flows using the Pom-Pom Model and Higher-Order Finite Volume Schemes" Report # CSR 6-2005, UNIVERSITY OF WALES SWANSEA, 2005.